IEEE Access
Multidisciplinary ⋮ Rapid Review ⋮ Open Access Journal

Received 6 June 2024, accepted 4 July 2024, date of publication 11 July 2024, date of current version 17 September 2024.

Digital Object Identifier 10.1109/ACCESS.2024.3427007

RESEARCH ARTICLE

Exploring Magnetic Tractor Beam Technology for Enhanced Catheter Steering: Insights From Simulation and Experimentation

CHAYABHAN LIMPABANDHU AND ZION TSZ HO TSE
Centre for Bioengineering, School of Engineering and Materials Science, Queen Mary University of London, E1 4NS London, U.K.

Corresponding author: Zion Tsz Ho Tse (z.tse@qmul.ac.uk)

This work was supported in part by the Academy of Medical Sciences Professorship, in part by the Royal Society Wolfson Fellowship, in part by the Cancer Research U.K. under Grant EDDPMA-Nov21\100026, in part by the National Institutes of Health (NIH) Bench-to-Bedside Award, in part by the NIH Center for Interventional Oncology under Grant ZID BC011242 and Grant CL040015, and in part by the Intramural Research Program of the National Institutes of Health.

ABSTRACT This study explores the optimisation of catheter navigation for minimally invasive medical procedures by determining the Magnetic Tractor Beam (MTB) effect. The investigation involves both experimental setups and COMSOL simulations. The main emphasis is placed on examining the impact of factors such as the co-lead magnet's quality, the follower magnet's size, and their arrangement in space on the effectiveness of MTB-based steering mechanisms. This research aims to identify critical variables that improve catheter navigation accuracy and manoeuvrability through experiments and advanced simulations. The simulation component is essential for analysing and understanding the complex magnetic interactions involved in the MTB effect. It enables an in-depth understanding of the magnetic fields and forces involved. The comparison of the experimental findings and simulation results shows that there is an average percentage error of 3.84%. This shows a correlation between the two, demonstrating that the simulations accurately predict the practical outcomes for MTB-based catheter navigation systems. The result confirms the reliability of simulations for the advancement and improvement of catheter navigation techniques and highlights the potential of MTB coupling as a considerable development in medical technology. This method can potentially enhance the safety, effectiveness, and results of catheter-based interventions, representing a significant advancement in the development of minimally invasive medical procedures.

INDEX TERMS Magnetic actuation catheter, magnetic navigation, magnetic navigation catheter, magnetic stimulation, steerable catheter.

I. INTRODUCTION

The implementation of catheter-based methods for minimally invasive lung procedures has had an impact on the field of respiratory treatment [1]. Clinicians can diagnose and treat various lung conditions, such as lung cancer, infections, and pleural effusions, with significantly less trauma to the patient by accessing the lungs through a catheter [2]. However, despite these advancements, there are still significant challenges when navigating the complex bronchial pathways. The ability to precisely insert a catheter is constrained by limited visibility and complications. This highlights the importance of enhancing accuracy and procedural stability. The development of advanced imaging and navigation technologies has played an essential part in addressing these challenges, marking the development of safer and more accurate research for lung interventions using catheters [3], [4]. These advancements demonstrate significant advancement [5], [6], [7], [8], promising a more accurate and safer approach to lung procedures using catheters, ultimately improving patient outcomes and reducing recovery times [9], [10].

Catheter navigation is one of the fundamental aspects of today's medical treatment, allowing for precise diagnostics, treatments, and interventions [11], [12], [13], [14], [15]. The limitations associated with conventional steering methods, such as manual manipulation, have led to investigating novel approaches to enhance flexibility, control, and accuracy [16],

The associate editor coordinating the review of this manuscript and approving it for publication was Chaitanya U. Kshirsagar.

[17]. The Magnetic Tractor Beam (MTB) coupling is a magnetic method that shows potential for improving catheter navigation [18]. Catheter steering, or the ability to navigate catheters precisely and efficiently through complex anatomical pathways, is a critical challenge in interventional treatments [19], [20]. Traditional catheters commonly experience limitations in flexibility and controllability when manipulated externally. The exploration of novel techniques resulted in the study of MTB effects to enhance catheter manoeuvrability and enable treatment approaches with remarkable accuracy.

Nevertheless, various methods are being studied to improve the manoeuvrability of catheters. Another significant magnetic approach involves using externally applied magnetic fields to manipulate the catheter [21], [22], [23]. This method involves generating a magnetic field outside the patient's body to control the movement of a catheter tip that acts to magnetic forces. It provides a high level of accuracy and reduces the requirement for physical exertion. Aside from magnetic methods, non-magnetic methods like robotic-assisted steering have become increasingly popular [24], [25], [26]. These systems provide precise control over the movement of a catheter, using real-time imaging to adjust with a level of accuracy that cannot be achieved through manual methods alone.

Magnetic simulation provides the basis for optimising the implementation of magnetic steering techniques, such as MTB and external magnetic field control, by improving the understanding of the magnetic interactions involved. This paper explores the magnetic interactions that drive MTB coupling while assessing the effectiveness of external magnetic fields in steering catheters. This study includes assessing MTB effects across various magnet grades and thicknesses using COMSOL simulation software to refine MTB design for improved navigation.

This paper also aims to study the MTB effects further, including the MTB distance in different thicknesses and grades of the magnet, and use the COMSOL simulation software to determine the MTB effects. The aim is to develop a novel approach to the MTB design, which allows responsive and adaptive catheter navigation within the human body by integrating magnetic fields within the catheter system and employing advanced control mechanisms, focusing on understanding the new magnetic interaction through simulation.

II. METHOD AND PROCEDURES

A. LIST OF MAGNETS USED

This paper consists of ninety-six magnets categorised into two experiments with three positions: Lead magnet, Co-lead magnet and Follower magnet. A list of magnets and their properties are provided in Table 1. Ninety-six magnets were chosen to represent a large but manageable number of configurations that could be systematically tested within our experimental setup. While the number holds no specific significance, it allowed various possible configurations to be explored to ensure comprehensive analysis and robustness in the results. The goal was to maximise the number of combinations tested within practical constraints.

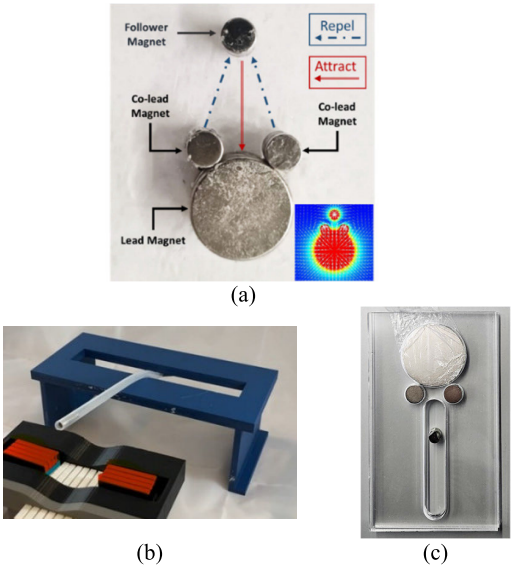

FIGURE 1. Example of MTB magnets with their concept. a) MTB magnets diagram with COMSOL simulation b) MTB catheter c) Example of Laser-cut pegboard with inverter magnet and follower magnet used in the experiment.

B. MAGNETIC TRACTOR BEAM (MTB) THICKNESS AND GRADE EXPERIMENT

An inverter magnet, often called an MTB magnet, comprises magnets that generate a single magnetic field. The principles behind catheter actuation are based on the current design of this inverter magnet (Fig. 1a). Adjusting the distance between co-lead magnets impacts the distance between the follower magnet and the inverter magnet; bringing the co-lead magnets closer results in the follower magnet moving further away from the inverter magnet, and conversely, increasing the separation between the co-lead magnets draws the follower magnet closer to the inverter magnet. This configuration allows users to effectively control the follower magnet's distance [18].

The follower magnet can be affixed to the catheter's distal end (Fig 1b), facilitating its application in various lung procedures. The inverter magnet, strategically employed to guide the catheter's tip, enhances its flexibility and manoeuvrability [18]. This configuration enables precise control over the catheter's movement, making it a valuable tool in lung interventions, where accuracy and adaptability are paramount.

The experiment aimed to investigate the MTB effect and involved the utilisation of diverse follower magnet sizes and thicknesses in combination with N42 and N52 grade co-lead magnets. This comprehensive approach allowed for examining distinctions between various combinations to understand the MTB effect better. The N52 magnet, known for its robust magnetic properties, was compared with the N42 magnet, which offered a favourable cost-performance ratio.

TABLE 1. List of magnets used in the experiment and their properties.

Experiment	Position	Size (mm)		Grade	Magnetic Flux Density ($\boldsymbol{B}$) (guass)	Magnetic Dipole Moment ($\boldsymbol{\mu}$) (Am^2)
		Diameter / Width x Length	Thickness			
MTB Thickness and Grade Experiment	Lead	50	20	N52	4623	46.2
	Co-Leads	15	20	N52	6929	4.16
	Follower	1 to 15	16, 18, and 20	N42	6180- 6,592	0.0527 - 3.71
COMSOL Model Experiment	Lead	50	20	N52	4623	46.2
	Co-Leads	15	20	N52	6929	4.16
	Follower	5	20	N52	7,330	0.416
	Follower	3	18	N52	7,374	0.150
	Follower	1 to 15	16, 18, and 20	N42	6180- 6,592	0.0527 - 3.71

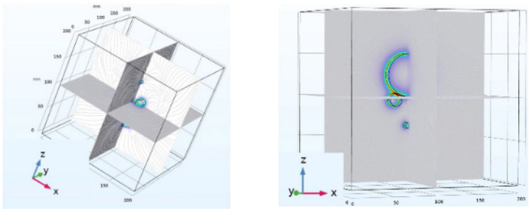

(a) (b)

FIGURE 2. Magnetic flux density distribution in different orientations of the magnets a) Horizontal Plane – when the magnet is placed horizontally, b) Vertically Upside-down Plane – when the magnet is placed vertically upside down.

The experimental methodology utilised SOLIDWORKS software to create designs and laser-cut pegboards to explore different distances between co-lead magnets. The design included a lead magnet with a diameter of 50 mm and two co-lead magnets with a diameter of 15mm. The distance between the co-lead magnets can be varied from 9 mm to 16 mm, an essential factor in studying the MTB effect. The study focused on the effects of magnet thickness and material grade by focusing on two specific pegboard spacings: 15mm and 16mm. The experiment includes using follower magnets with diameters ranging from 1 mm to 15 mm to determine the smallest practical size. Additionally, inverter magnets were tested in 20 mm and 10 mm thicknesses to determine their impact on the system. An example of a pegboard with an experimental setup can be found in Figure 1c.

In addition, the experiment examined how the distances between the lead and follower magnets, for both inverter magnet thicknesses, affected the system's behaviour. This was done by placing each magnet in the holes of the pegboard and measuring the distance from one magnet to another by measuring the distance between their edges. The measurements were specifically altered to account for various follower magnet thicknesses and different co-lead magnet grades. A novel aspect of the study assessed gravity's impact on the follower magnet's functionality by placing the pegboard in a vertically upside-down position. The objective of this setup was to observe the potential levitation of the follower magnet and better understand the net forces present as a consequence of gravitational influence.

The experimental procedures featured safety measures and guidelines to address the raised concerns about safety and proper execution, thereby ensuring the integrity and well-being of everyone involved. Before initiating the experiments, researchers received specialised safety training for handling powerful magnetic fields and precision laser-cut materials. In addition, the experiment's design included fail-safe mechanisms to rapidly demagnetise the setup in an emergency, thereby reducing the risks associated with unexpected movements in the magnetic field. The precautions were carefully recorded and followed, ensuring that the study of the MTB effect using different magnet configurations was carried out in a controlled and secure manner.

C. MODEL EXPERIMENT

A magnetic simulation was developed using the COMSOL Multiphysics software (Stockholm, Sweden) to analyse magnetic interactions extensively. This simulation focused on a 'Magnetic Fields, No Currents (mfnc)' study using the 'Stationary' solver category. The objective was to analyse the magnetic flux density and force distribution among a specific arrangement of N42 and N52 grade sintered NdFeB magnets. The arrangement of these magnets was essential to the simulation, representing two experimental setups that included a total of 96 magnets. These magnets were placed in three locations to explore their interactions using finite element analysis (FEA). The outcomes of these simulations were represented in a three-dimensional (3D) domain to offer an in-depth analysis of the magnetic field configurations. Furthermore, a strategic 2D cross-section taken through the centre of the magnet array provided data about the magnetic flux density at that specific location.

Figure 2 illustrates the magnetic flux density distribution in horizontal and vertical planes passing through the magnets. These planes were selected to provide a detailed view of the magnetic field interactions within different orientations of the magnet setup. The horizontal plane shows the flux density distribution when the magnet is placed horizontally, considering the x-axis and z-axis. The vertical plane presents the distribution when the magnet is placed vertically upside down, considering all axes (x, y, and z).

Moreover, the computation of the net force ($\boldsymbol{F}$) exerted on the Follower Magnet involves utilising the ''Force Calculation node' within the 'Magnetic Fields, No Currents (mfnc)' studies. The net force ($\boldsymbol{F}$), Torque ($\boldsymbol{\tau}$) and Torque axis ($\boldsymbol{\tau_{\alpha x}}$) can be calculated by using the equation (1) - (3):

$$F = \int_{\partial\Omega}^{\tau_0} nT \, ds \tag{1}$$

TABLE 2. Material properties of magnets used in the simulation.

Property	Expression
Relative permittivity	1
Recoil permeability	1.05
Electrical conductivity	1/1.4 uΩ · m
Remanent flux density norm	1.44 T

$$\tau = \int_{\partial\Omega}^{\tau_0} (r - r_0) \times (nT) dS \tag{2}$$

$$\tau_{\alpha x} = \frac{r_{\alpha x}}{|r_{\alpha x}|} \cdot \tau \tag{3}$$

where $\boldsymbol{n}$ is the normal pointing out from the domain containing material, $\boldsymbol{T}$ is the stress tensor, $\boldsymbol{S}$ is the solid boundary, $\boldsymbol{r}$ denotes the coordinates of a material point, torque axis in vector ($\boldsymbol{r_{\alpha x}}$) is equal to $\begin{bmatrix} \mathbf{0} \\ \mathbf{1} \\ \mathbf{0} \end{bmatrix}$ and torque rotation point ($\boldsymbol{r_0}$) is equal to $\begin{bmatrix} \mathbf{0} \\ \mathbf{0} \\ \mathbf{0} \end{bmatrix}$.

D. MTB ON A HORIZONTAL PLANE

In this simulation, the magnets are assumed to be positioned on a horizontal plane (XZ-plane), with the Y-plane (vertical plane) disregarded since the magnets remain fixed along that axis. Table 2 provides a comprehensive list of the magnet properties employed in this simulation. To determine the magnetic flux density norm, a 2D plane is intersected through the centre of all magnets within the 3D plane where the simulation results were obtained. Additionally, the net force exerted on the Follower Magnet is calculated. The simulation maintains a fixed distance of 15 mm and 16 mm between co-lead magnets, a value confirmed through experimentation in the MTB Thickness and Grade Experiment as the critical distance for activating the MTB effect. In this simulation, the Follower Magnet's position ranges from close proximity to the lead magnet to a considerable distance, encompassing both sides of the co-lead magnets.

E. MTB ON A VERTICALLY UPSIDE-DOWN PLANE

The magnets are inverted vertically, and the follower magnet is below the inverter magnet, introducing gravity into the equation through the 'Solid Mechanics' studies. This adjustment considers the XYZ plane in the simulation, as the magnetic forces are affected by the magnets being turned upside down. In this simulation, the inverter magnet remains stationary, with the magnetic properties of the simulated magnets detailed in Table 3. Gravity acting on the magnet is taken into account in the simulation on the vertically upside-down plane setup. Following this reconfiguration, the same methodologies employed in the previous simulation derive the magnetic flux density norm and the net force acting on the Follower Magnet. The simulation maintains a fixed distance of 16 mm between co-lead magnets, a value

TABLE 3. Material properties of magnets used in the simulation.

Property	Expression
Relative permittivity	1
Recoil permeability	1.05
Density	7400 kgm^{-3}
Young's modulus	160000000000 Pa
Electrical conductivity	1/1.4 uΩ · m
Poisson's ratio	0.24
Remanent flux density norm (N52 Magnets)	1.44 T

substantiated by the MTB Thickness and Grade Experiment findings, which identify 15mm and 16mm as the activation distance for the MTB effect. Additionally, the Follower Magnet's position varies from proximity to the lead magnet to considerable distances and different alignments that deviate from direct alignment with the inverter magnet along the Y plane.

F. EXPERIMENTAL RESULT VS. SIMULATION RESULT

The MTB Thickness and Grade Experiment results are utilised to deepen the analysis of the MTB magnet simulation. This experiment compared the experimental distance between the Lead and Follower Magnet with the simulation results obtained through COMSOL. However, in the experiment, the follower magnet was N42 grade. An adjustment in the simulation was then made by altering the 'Remanent Flux Density Norm' within the material properties of the Follower Magnet, transitioning from 1.44 T to 1.31 T, thus resulting in the simulated magnet more closely matching the experimental magnet.

The comparison involved calculating the percentage error between the experimentally measured distance and the simulated distance between the follower and lead magnets. The average percentage error for each magnet size and the overall average percentage error were calculated for a comprehensive analysis.

III. RESULT AND DISCUSSION

A. MAGNETIC TRACTOR BEAM (MTB) DISTANCE

Figure 3 reveals a significant correlation: an increase in the follower magnet's size leads to a reduced gap between it and the lead magnet. Thickness is crucial in the MTB effect, particularly when the pegboard is vertically inverted. If the follower magnet's thickness matches the inverter magnet's (20mm), the MTB effect fails. This is due to the influence of gravity, disrupting the magnet's equilibrium necessary for the MTB effect. The most stable MTB effect occurs when the follower magnet's thickness aligns with 16mm. The following equation summarises this phenomenon:

$$F_{thickness} < L_{thickness}$$
$$L_{thickness} = Co - L_{thickness}$$

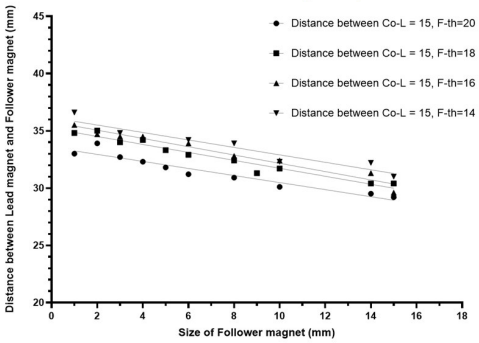

(a)

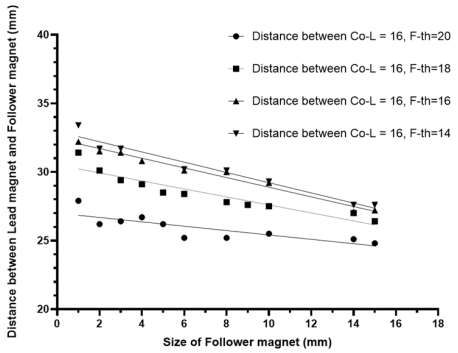

(b)

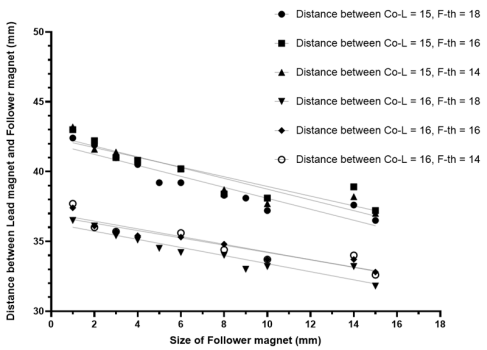

(c)

FIGURE 3. Distance between the lead magnet and follower magnet, where Co-L=Co-lead magnets, and F-th = Follower magnet's thickness, and the values of Co-L and F-th are in mm. The standard deviation is plotted in the graph as an error bar. (a) pegboard placed horizontally where the distance between Co-lead is 15mm (b) pegboard placed horizontally where the distance between Co-lead is 16mm (c) pegboard placed vertically upside down.

Figures 3 and 4 confirm a significant trend: larger inverter magnets enable increased separation between lead and follower magnets. Curve-fitting results indicate an inverse relationship between these magnets' distance and co-lead magnets' proximity. Figure 4 highlights that using N42 co-lead magnets reduces the distance between lead and follower magnets due to N42's weaker magnetic field than N52.

Larger follower magnets amplify attraction forces while co-lead magnet repulsion remains constant, reducing the separation between lead and follower magnets. Moreover, when comparing two experiments in Figures 3 and 4, varying the inverter magnet thickness (10 mm to 20 mm) affects

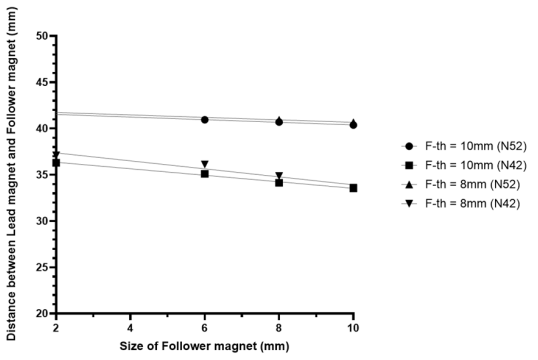

(a)

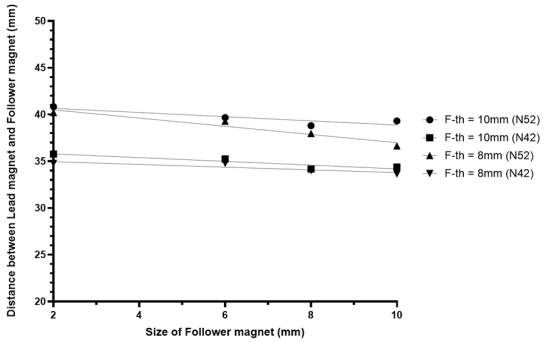

(b)

FIGURE 4. Distance between the lead magnet and the follower magnet, where the pegboard is only placed horizontally, and F-th = thickness of the follower magnet, all in mm. The standard deviation is plotted in the graph as an error bar. (a) distance between Co-lead is 15mm (b) distance between Co-lead is 16mm.

the distance between the magnets. Thinner inverter magnets increase separation, whereas thicker ones enhance MTB stability. Notably, the distance graph slope remains uniform with constant follower magnet grade and co-lead magnet distance.

B. COMSOL MODEL EXPERIMENT

1) MTB ON A HORIZONTAL PLANE

Figure 5 illustrates a series of simulations involving the inverter magnet and follower magnets in various scenarios. At the same time, Table 4 provides a detailed account of the net force results affecting the follower magnet under these conditions and the distance between the follower magnet and the lead magnet from edge to edge. When the follower magnet is close to the inverter magnet, the repulsion force from the co-lead magnets becomes ineffective, and the attractive force from the lead magnet overpowers any repulsion. Consequently, the follower magnet is drawn closer to the lead magnet. The degree of attraction determines the proximity of the follower magnet to the lead magnet, as evident in Figures 5a and 5b. In scenarios where the repulsion force starts to act on the follower magnet, even when it is not precisely in the MTB effect position, a stronger repulsion force propels the follower magnet upward, bringing it closer to the inverter magnet. This is exemplified in Figures 5c and 5d.

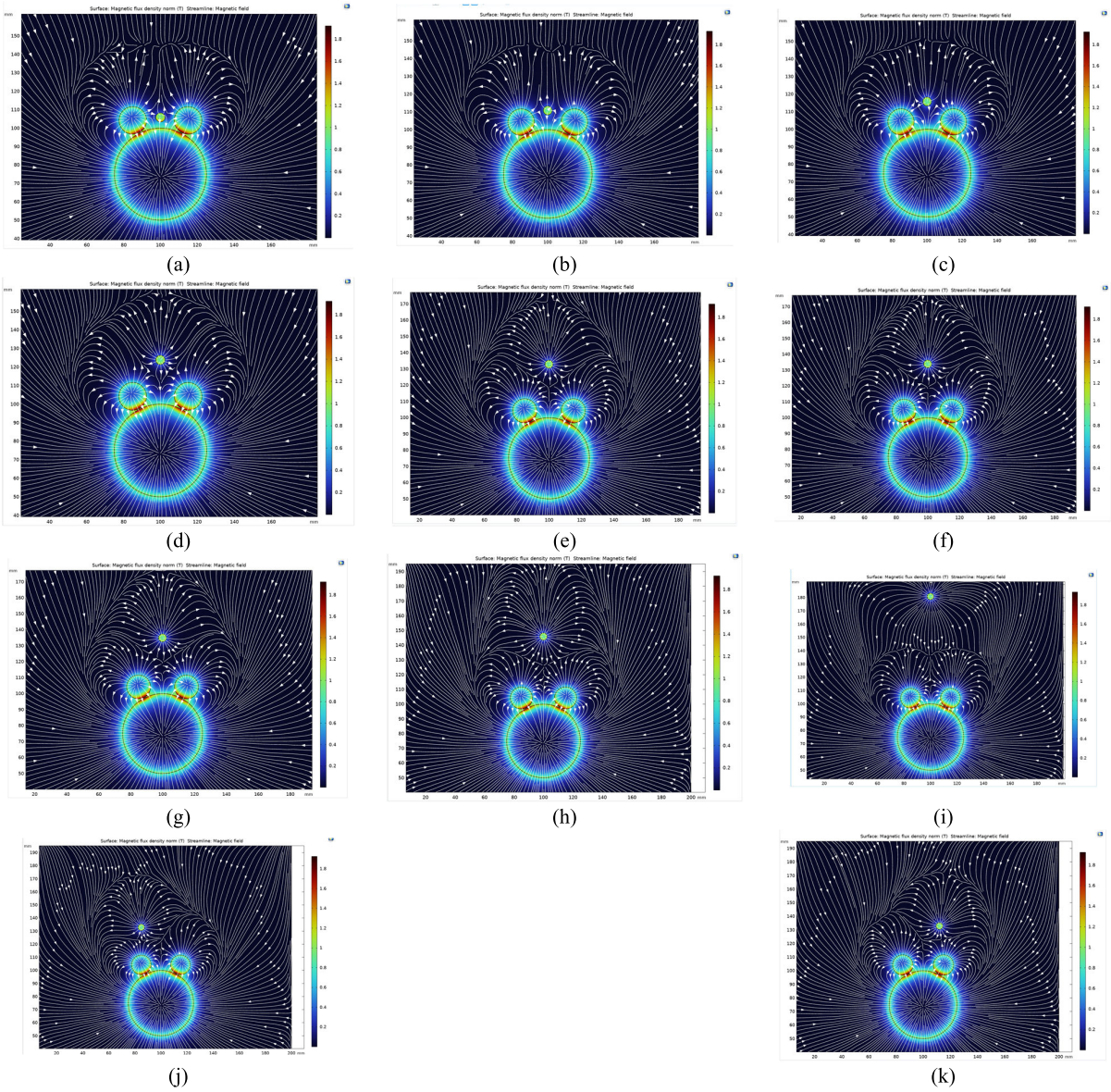

FIGURE 5. Inverter and follower magnets in different scenarios on the horizontal plane. The arrows show the magnetic flux directions between the four magnets.

TABLE 4. Follower magnet's net force on a horizontal plane.

Figure	Follower magnet's Position		Follower magnet's Net force	
	X	Z	X	Z
Figure 5a	0.0	5.8	0.0	-12.5
Figure 5b	0.0	10.8	-0.1	-0.9
Figure 5c	0.0	15.8	0.1	1.1
Figure 5d	0.0	23.8	-0.1	0.6
Figure 5e	***0.0***	***32.9***	***0.0***	***0.0***
Figure 5f	0.0	33.9	-0.1	-0.2
Figure 5g	0.0	34.9	-0.1	-0.1
Figure 5h	0.0	45.9	0.1	0.2
Figure 5i	0.0	80.9	0.0	0.0
Figure 5j	-15.0	32.9	0.0	0.3
Figure 5k	12.0	32.9	0.1	0.1

The MTB effect creates an air gap between the magnets, causing the follower magnet to reach an equilibrium state where it neither moves closer nor further away from the inverter magnet. As the simulation solely evaluates forces in

TABLE 5. Follower magnet's net force on a vertically upside-down plane.

Figure	Follower magnet's Position			Follower magnet's Net force		
	X	Y	Z	X	Y	Z
Figure 6a	0.0	0.0	10.0	0.1	0.0	3.0
Figure 6b	0.0	0.0	31.6	0.1	0.0	-0.6
Figure 6c	***0.0***	***0.0***	***35.6***	***0.0***	***0.0***	***0.0***
Figure 6d	0.0	0.0	37.6	0.1	0.0	0.2
Figure 6e	0.0	0.0	39.6	0.0	-0.1	-0.4
Figure 6f	0.0	0.0	44.0	-0.2	-0.2	0.3
Figure 6g	0.0	0.0	70.6	0.0	-0.1	-0.1
Figure 6h	0.0	-6.0	35.6	0.1	-0.1	0.0
Figure 6i	0.0	10.0	35.6	0.1	-0.1	-0.1
Figure 6j	-15.5	0.0	35.6	0.0	0.1	-0.3
Figure 6k	20.0	0.0	35.6	-0.3	0.2	-0.2
Figure 6l	-8.0	10.0	35.6	0.2	0.1	-0.2

static conditions, the net force acting on the follower magnet during the MTB effect position equals zero. The MTB effect operates within specific distances where the net force in the x and z planes is balanced, as depicted in Figure 5e. When the follower magnet is close to the MTB effect position but not precisely aligned, the lead magnet exerts a slight force, drawing it to the MTB effect position. The strength of this force determines the proximity, as seen in Figures 5f and 5g. However, suppose the follower magnet is too distant from the lead magnet (Figure 5h). In that case, the repulsion force from the co-lead magnets prevails, potentially causing the follower magnet to move away. Alternatively, when the follower magnet is far from the inverter magnet (Figure 5i), no significant force acts on it, and the net force returns to zero. In this case, the follower magnet does not move in tandem with the inverter magnet.

Additionally, when the follower magnet is aligned with the centre of one of the co-lead magnets, it experiences the repulsion force from that specific co-lead magnet, propelling it upward along the centreline shared by both magnets (Figure 5j). However, if the follower magnet is not precisely aligned with the centre of the inverter magnet, one of the co-lead magnets may overcome the attraction force of the lead magnet, causing the follower magnet to move away to one side, influenced by the specific co-lead magnet's repulsion force (Figure 5k). It's important to note that when the follower magnet moves away, there's a possibility it may be attracted to the lead magnet at a different angle, where the repulsion force from the co-lead magnets no longer affects its trajectory.

2) MTB ON A VERTICALLY UPSIDE-DOWN PLANE

Figure 6 comprehensively depicts the simulation involving an inverter magnet and follower magnets on a vertically upside-down plane. Table 5 offers insights into the net force outcomes affecting the follower magnet in various scenarios, as detailed in Figure 6. It also shows the distance between the follower and lead magnets from edge to edge. Due to its vertically upside-down orientation, this unique setup allows the follower magnet to move freely within a 360-degree range across the X, Y, and Z planes. In Figure 6a, when the follower magnet is close to the lead magnet, the attractive force from the lead magnet surpasses both the force of gravity and the repulsion from the co-lead magnets, leading to the attraction of the follower magnet by the lead magnet. As shown in Figure 6b, when the follower magnet is near the MTB effect position but close to the inverter magnet, it experiences a downward movement driven by the combined repulsion force from the co-lead magnets and gravity, ultimately positioning it within the MTB effect range.

Figure 6c depicts the MTB effect position, where the follower magnet reaches an equilibrium state, levitating without any motion and maintaining a net force of zero, similar to the scenario shown in Figure 6f. In situations where the inverter magnet moves, the follower magnet maintains a fixed distance from the lead magnet, as displayed in Figure 6c. For scenarios where the follower magnet is not in the MTB effect position, it is drawn upward towards the MTB effect position if the Tools and equipment repulsion force and gravity do not surpass the attraction force from the lead magnet, as seen in Figure 6d.

Figures 6e, 6f, and 6g reveal that when the follower magnet is located too far from the inverter magnet, beyond the effective range of the lead magnet's attraction, it may fall due to the influence of gravity and the repulsion force. Alternatively, it might fly away, seeking attraction from the lead magnet in a different area. However, suppose the centre of the follower magnet is not aligned with the centre of the inverter magnet in the Y-plane. In that case, it will be propelled away and subsequently attracted by the lead magnet in an alternative region, as depicted in Figures 6h and 6i. Moreover, when the position of the follower magnet is situated on either side of the co-lead magnet, not aligned with the centre in the X-plane, the follower magnet's behaviour varies depending on its location and the resultant net force acting upon it, as seen in Figure 6j and 6k. Figure 6l depicts a situation in which the follower magnet is not correctly

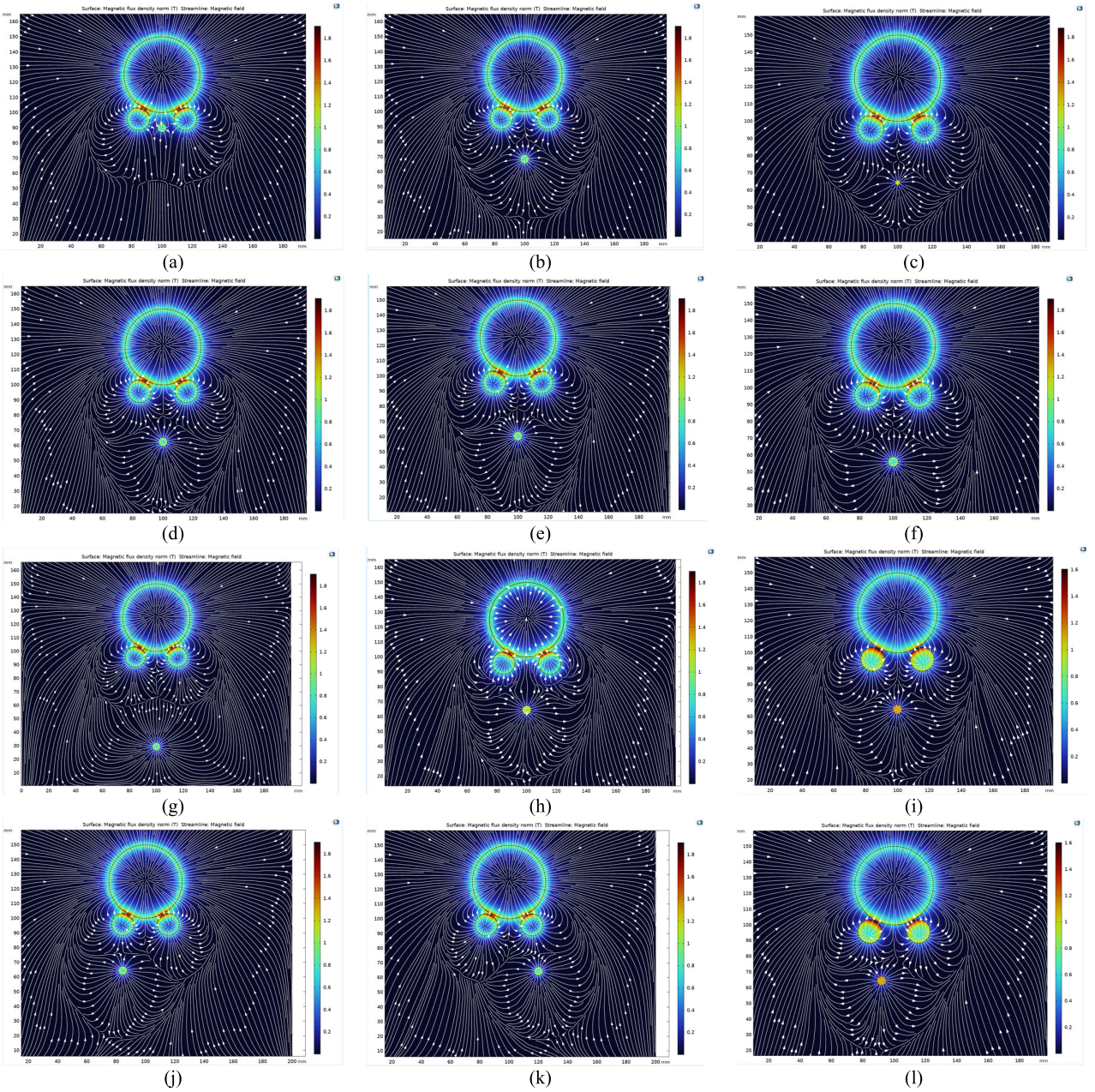

FIGURE 6. Inverter and follower magnets in different scenarios on the vertically upside-down plane.

positioned in both the X and Y planes. The follower magnet behaves unsteadily in this situation, perhaps swerving away predictably depending on its position.

The primary focus in the presented scenarios was on analysing static simulation results to gain an in-depth understanding of the complexities of the MTB effect under different conditions. These simulations explain how the positions and distances between the follower, lead, and co-lead magnets affect the system's behaviour in a controlled and stationary environment. Although these findings are valuable for theoretical analysis and initial understanding, they serve primarily as a foundation for research and require further research into dynamic behaviours.

To gain practical applications and a thorough comprehension of the MTB effect, it is essential to broaden the research to include dynamic motion simulations and evaluations of variations in time in forces caused by magnet movement. This method would accurately depict real-life situations in which magnets experience continuous movement and varying external influences. Furthermore, it is imperative to examine the stability of these static findings. The process entails analysing how slight modifications in experimental factors, such as the position or orientation of a magnet or the presence of external forces, can result in significant variations in the behaviour and dynamics of the magnet's force. Conducting a thorough analysis at an additional level is essential for

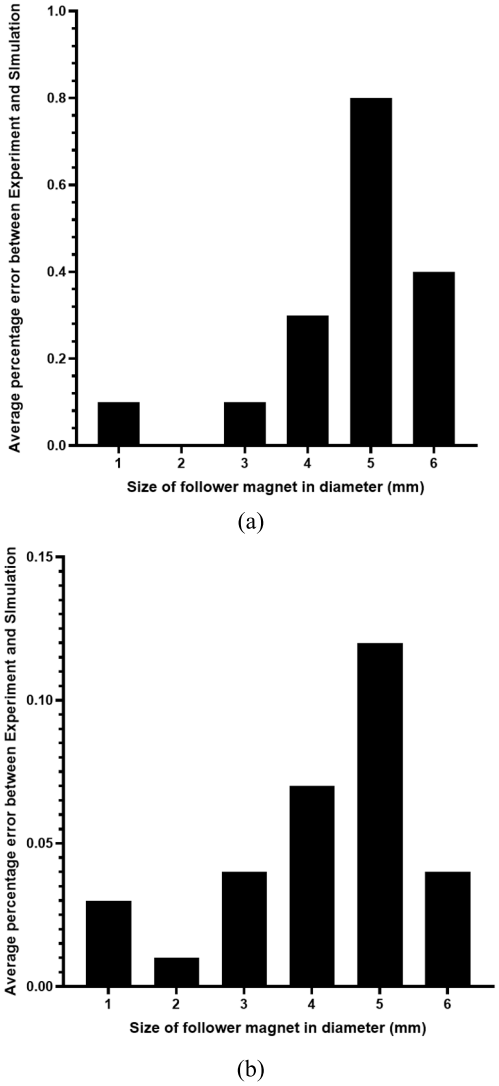

FIGURE 7. The error percentage in the distance between lead and follower magnet results was compared between the experiment and simulation. a) Average percentage error of each magnet size in the horizontal plane b) Average percentage error of each magnet size in the vertically upside-down plane.

ensuring the reliability and relevance of the MTB effect in real-life situations, where accurate control and predictable results are of the highest priority.

3) PERCENTAGE ERROR BETWEEN EXPERIMENTAL RESULT AND SIMULATION RESULT

The result from the MTB thickness and graded experiment is used to compare the result in this section, where the percentage error between the two similar scenarios is calculated. Figure 7, which represents the percentage difference between our experimental and COMSOL simulation results, is an integral part of our analysis. Notably, the distance measurements between the lead and follower magnets in the experiment and simulation are highly similar, with only a minor difference. This minor difference could be attributed to the inherent possibility of human error during the experimental phase.

The exceptional level of precision, as demonstrated by the deficient total percentage error of 2 %, is essential. This insignificant value illustrates the experiment's precision and dependability, indicating an exceptionally high level of accuracy in both experimental and simulation results. Moreover, the close result of the distances between the lead and follower magnets with such a small percentage error demonstrates the consistency of the results. It validates simulation and highlights the potential for MTB effects to improve precision in medical interventions.

While the COMSOL simulation package is well-validated, and its agreement with experimental measurements is anticipated, this study verifies the effects of the thickness and size of the follower magnets. This approach ensures that the findings are robust and reliable. Combining simulation and experimental methods offers a comprehensive analysis that confirms the consistency and accuracy of the results across different verification techniques.

IV. CONCLUSION

The study delves into MTB coupling and its impact on catheter steering. It reveals crucial factors influencing lead-follower magnet distances, notably their inverse relationship with co-lead magnet spacing. Variances in co-lead magnet grades, such as N42 and N52, affect performance. The follower magnet's size, diameter, and thickness play a pivotal role in attraction and repulsion forces, shaping the distance between magnets.

The study highlights how co-lead magnet proximity affects spatial arrangements. As co-lead magnets draw nearer, the lead-follower magnet gap widens. The thickness of the inverter and follower magnets emerges as a critical factor. Thinner magnets increase the lead-follower distance, while thicker ones promote a stable MTB effect. These findings emphasise the intricate interplay of forces and magnet attributes in catheter navigation, offering promise for precision in medical interventions.

Moreover, the research underscores the remarkable potential of the MTB effect. It achieves consistent results with minimal divergence between experiments and COMSOL simulations, primarily attributed to minor experimental errors. The study demonstrates extraordinary precision, with a total percentage error of 2 %, affirming the reliability of experimental procedures and simulation accuracy. The proximity of lead-follower magnet distances and low percentage errors validate MTB's potential to enhance precision in various applications, particularly in medical interventions. Given the remarkable alignment between the simulation results and the corresponding experimental data, it is reasonable to conclude that simulations can be conducted effectively without an experimental setup. This implies that additional simulation tests can be performed before constructing a prototype system.

REFERENCES

[1] C. Chautems, A. Tonazzini, Q. Boehler, S. H. Jeong, D. Floreano, and B. J. Nelson, "Magnetic continuum device with variable stiffness for minimally invasive surgery," *Adv. Intell. Syst.*, vol. 2, no. 6, Jun. 2020, Art. no. 1900086.
[2] J. R. Rojas-Solano, L. Ugalde-Gamboa, and M. Machuzak, "Robotic bronchoscopy for diagnosis of suspected lung cancer: A feasibility study," *J. Bronchol. Interventional Pulmonol.*, vol. 25, no. 3, pp. 168–175, 2018.
[3] S. M. Jeon and G. H. Jang, "Precise steering and unclogging motions of a catheter with a rotary magnetic drill tip actuated by a magnetic navigation system," *IEEE Trans. Magn.*, vol. 48, no. 11, pp. 4062–4065, Nov. 2012.
[4] V. N. T. Le, N. H. Nguyen, K. Alameh, R. Weerasooriya, and P. Pratten, "Accurate modeling and positioning of a magnetically controlled catheter tip," *Med. Phys.*, vol. 43, no. 2, pp. 650–663, Feb. 2016.
[5] Z. Yang, L. Yang, M. Zhang, C. Zhang, S. C. H. Yu, and L. Zhang, "Ultrasound-guided catheterization using a driller-tipped guidewire with combined magnetic navigation and drilling motion," *IEEE/ASME Trans. Mechatronics*, vol. 27, no. 5, pp. 2829–2840, Oct. 2022, doi: 10.1109/TMECH.2021.3121267.
[6] T. Liu, R. Jackson, D. Franson, N. L. Poirot, R. K. Criss, N. Seiberlich, M. A. Griswold, and M. C. Çavusoglu, "Iterative Jacobian-based inverse kinematics and open-loop control of an MRI-guided magnetically actuated steerable catheter system," *IEEE/ASME Trans. Mechatronics*, vol. 22, no. 4, pp. 1765–1776, Aug. 2017.
[7] C. Eitel, G. Hindricks, M. Grothoff, M. Gutberlet, and P. Sommer, "Catheter ablation guided by real-time MRI," *Current Cardiol. Rep.*, vol. 16, no. 8, p. 511, Aug. 2014.
[8] L. Müller, M. Saeed, M. W. Wilson, and S. W. Hetts, "Remote control catheter navigation: Options for guidance under MRI," *J. Cardiovascular Magn. Reson.*, vol. 14, no. 1, p. 43, Jan. 2012.
[9] Z. Zhao, S. Jordan, and Z. T. H. Tse, "Devices for image-guided lung interventions: State-of-the-art review," *Proc. Inst. Mech. Eng., H, J. Eng. Med.*, vol. 233, no. 4, pp. 444–463, Apr. 2019.
[10] M. P. Armacost, J. Adair, T. Munger, R. R. Viswanathan, F. M. Creighton, D. T. Curd, and R. Sehra, "Accurate and reproducible target navigation with the stereotaxis Niobe magnetic navigation system," *J. Cardiovascular Electrophysiology*, vol. 18, no. s1, pp. S26–S31, Jan. 2007.
[11] J. Hwang, J.-Y. Kim, and H. Choi, "A review of magnetic actuation systems and magnetically actuated guidewire- and catheter-based microrobots for vascular interventions," *Intell. Service Robot.*, vol. 13, no. 1, pp. 1–14, Jan. 2020.
[12] M. Wobith, L. Wehle, D. Haberzettl, A. Acikgöz, and A. Weimann, "Needle catheter jejunostomy in patients undergoing surgery for upper gastrointestinal and pancreato-biliary cancer–impact on nutritional and clinical outcome in the early and late postoperative period," *Nutrients*, vol. 12, no. 9, p. 2564, Aug. 2020.
[13] U. Chaddha, D. K. Hogarth, and S. Murgu, "Bronchoscopic ablative therapies for malignant central airway obstruction and peripheral lung tumors," *Ann. Amer. Thoracic Soc.*, vol. 16, no. 10, pp. 1220–1229, Oct. 2019.
[14] T. Liu, N. Lombard Poirot, T. Greigarn, and M. C. Çavuşoğlu, "Design of a magnetic resonance imaging guided magnetically actuated steerable catheter," *J. Med. Devices*, vol. 11, no. 2, Jun. 2017.
[15] Y. Fu, H. Liu, W. Huang, S. Wang, and Z. Liang, "Steerable catheters in minimally invasive vascular surgery," *Int. J. Med. Robot. Comput. Assist. Surg.*, vol. 5, no. 4, pp. 381–391, Dec. 2009.
[16] X. Hu, A. Chen, Y. Luo, C. Zhang, and E. Zhang, "Steerable catheters for minimally invasive surgery: A review and future directions," *Comput. Assist. Surg.*, vol. 23, no. 1, pp. 21–41, Jan. 2018.
[17] Z. Yang and L. Zhang, "Magnetic actuation systems for miniature robots: A review," *Adv. Intell. Syst.*, vol. 2, no. 9, Sep. 2020, Art. no. 2000082.
[18] C. Limpabandhu, Y. Hu, H. Ren, W. Song, and Z. Tse, "Towards catheter steering using magnetic tractor beam coupling," *Proc. Inst. Mech. Eng., H, J. Eng. Med.*, vol. 236, no. 4, pp. 583–591, Apr. 2022.
[19] C. Limpabandhu, Y. Hu, H. Ren, W. Song, and Z. T. Ho Tse, "Magnetically steerable catheters: State of the art review," *Proc. Inst. Mech. Eng., H, J. Eng. Med.*, vol. 237, no. 3, pp. 297–308, Mar. 2023.
[20] C. Limpabandhu, Y. Hu, H. Ren, W. Song, and Z. T. H. Tse, "Actuation technologies for magnetically guided catheters," *Minimally Invasive Therapy Allied Technol.*, vol. 32, no. 4, pp. 137–152, Aug. 2023.
[21] A. W. Mahoney and J. J. Abbott, "Managing magnetic force applied to a magnetic device by a rotating dipole field," *Appl. Phys. Lett.*, vol. 99, no. 13, Sep. 2011, Art. no. 134103.
[22] J. Sikorski, A. Denasi, G. Bucchi, S. Scheggi, and S. Misra, "Vision-based 3-D control of magnetically actuated catheter using BigMag—An array of mobile electromagnetic coils," *IEEE/ASME Trans. Mechatronics*, vol. 24, no. 2, pp. 505–516, Apr. 2019.
[23] J. Sikorski, C. M. Heunis, F. Franco, and S. Misra, "The ARMM system: An optimized mobile electromagnetic coil for non-linear actuation of flexible surgical instruments," *IEEE Trans. Magn.*, vol. 55, no. 9, pp. 1–9, Sep. 2019.
[24] G. Srimathveeravalli, T. Kesavadas, and X. Li, "Design and fabrication of a robotic mechanism for remote steering and positioning of interventional devices," *Int. J. Med. Robot. Comput. Assist. Surg.*, vol. 6, no. 2, pp. 160–170, Jun. 2010.
[25] P. M. Loschak, A. Degirmenci, C. M. Tschabrunn, E. Anter, and R. D. Howe, "Automatically steering cardiac catheters in vivo with respiratory motion compensation," *Int. J. Robot. Res.*, vol. 39, no. 5, pp. 586–597, Apr. 2020.
[26] J. J. Zhou, A. Quadri, A. Sewani, Y. Alawneh, R. Gilliland-Rocque, C. Magnin, A. Dueck, G. A. Wright, and M. A. Tavallaei, "The CathPilot: A novel approach for accurate interventional device steering and tracking," *IEEE/ASME Trans. Mechatronics*, vol. 27, no. 6, pp. 5812–5823, Dec. 2022.

CHAYABHAN LIMPABANDHU received the Bachelor of Engineering degree in electronics and communication engineering from the Sirindhorn International Institute of Technology, Thammasat University, and the Master of Science degree in intelligence systems and robotics from the University of Essex. She is currently pursuing the Ph.D. degree in medical engineering with the Digital Health and Robotics Laboratory, Queen Mary University of London, with a focus on magnetically actuated devices for medical interventions. Her academic journey and professional experiences are deeply rooted in the advancement of medical device technology, particularly in the integration of robotics and magnetic actuation in healthcare applications. Her contributions to interdisciplinary projects and academic competitions highlight her dedication to innovation in the fields of digital health and medical engineering.

ZION TSZ HO TSE received the Ph.D. degree in mechatronics in medicine from Imperial College London, U.K. He is currently an Academy of Medical Sciences Professor of digital health and robotics and the Director of the Centre for Bioengineering, Queen Mary University of London. Before that, he was a Chair Professor with the University of York and an Associate Professor with the University of Georgia. Before that, he was a Research Fellow with Harvard University, Boston, MA, USA. Most of his academic and professional experience has been in AI, digital health, medical robotics, and imaging. He has been developing and testing a broad range of medical technologies in his career, most of which have been applied in clinical patient trials. His research bridges engineering and medicine, connecting multidisciplinary teams of medical doctors, researchers, and engineers.